Hindawi
Mathematical Problems in Engineering
Volume 2020, Article ID 3718174, 16 pages
https://doi.org/10.1155/2020/3718174

Research Article

The Optimization Research of Diesel Cylinder Gasket Parameters Based on Hybrid Neutral Network and Improved Grey Wolf Algorithm

Yi Dong,[1] Jianmin Liu,[1] Yanbin Liu,[1] Xinyong Qiao,[1] Xiaoming Zhang,[1] Qi Kang,[2] and Tianqi Wang[1]

[1]*Vehicle Engineering Department, Army Academy of Armored Forces, Beijing 100072, China*
[2]*China Satellite Maritime Tracking and Controlling Department, Jiangyin 214431, China*

Correspondence should be addressed to Yanbin Liu; aafelyb@163.com

Received 6 July 2020; Revised 18 September 2020; Accepted 28 September 2020; Published 10 October 2020

Academic Editor: Diyuan Li

In order to improve reliability and fatigue life of cylinder gaskets in heavy duty diesel engine, several methods and algorithms are applied to optimize operating factors of gaskets. Finite element method is utilized to figure out and analyze the temperature fields, thermal-mechanical coupling stress fields, and deformations of gasket. After determining the maximum values of three state parameters, the orthogonal experimental design method is adopted to analyze the influence rules of five operating factors on three state parameters of the gaskets and four factors which most significantly affect these state parameters are determined. Then, the method which uses operating factors to predict state parameters is established on the application of hybrid neuron network based on partial least squares regression and deep neural network. The comparison results between the predicted values and real values verified the accuracy of the hybrid neuron network method. Based on artificial bee colony algorithm, improvement is attached to the way three kinds of grey wolves locate preys in grey wolf algorithm and the way how using different hierarchy wolfs in grey wolf algorithm to determine three weight coefficients and the location of prey is put forward with. The method using artificial bee colony algorithm to optimize the grey wolf algorithm is called ABC and GWO. The proposed HNN and the ABC and GWO method are applied to work out operating factors values which correspond to optimal state parameters of gasket, and the gaskets are optimized according to the optimal values. It has been demonstrated by finite element analysis results that maximum temperature, maximum coupling stress, and the maximum deformation decrease to 6 K, 12.57 MPa, and 0.0925 mm compared to the original values, respectively, which proves the accuracy of the algorithm and the validity of the improvement.

1. Introduction

Cylinder gaskets are critical to reliable sealing and stable operating of diesel engine. However, they are not only subjected to the scour from high-temperature gas, but also subjected to the pressure of cylinder heads, bodies, and the bolt preload forces during operation, the operating environment of which is very harsh. The area between the coolant flow channel and the combustor especially should bear not only the heat transfer from high-temperature gas and the heat dissipation of coolant, but also the explosive pressure and the bolt preload. In consequence, it is much likely for the gaskets to suffer fatigue damage failure. Thus, the detailed research on the temperature, stress, and deformation of the area mentioned is significant for ensuring the safe and reliable work of gaskets so as to improve the reliability and the performance index of diesel engine.

There are many researches which focus on the diesel engine and its high-temperature components, the research subject including combustion [1], engine performance [2], injection [3], fault diagnosis [4], mixture fuel [5], and waste heat recovery [6]. Kumar et al. [7] investigated the performance (emission and quality of the fuel) of engine using the diesel alcohol blend as the fuel. To compare the

difference of the fuel, they conducted a series of experiment in different situations to observe the performance of engine, including different operating load, different fuel component, and different operating speed. Results show that the diesel alcohol blend fuel has a better performance than other fuels and that methanol has a better emission performance than other fuels. Wei et al. [8] researched the problem about soot properties and its generating process. They investigated the macroscopic shape, nanostructure, and thermophysical properties of the soot. Results show that dimethyl carbonate diesel blends can generate smaller soot than other fuels and that macroscopic shape has less influence than nanostructure on the soot generation process. Subramaniam et al. [9] studied the properties of algae blend fuel and used the single cylinder diesel engine to do the experiment about the fuel. The experimental condition includes various algae volume, and the output parameters to be compared are thermal efficiency of engine, fuel consumption per unit output power, temperature of exhaust, and some properties of combustion. Results show that A20 has the better properties than the other blend fuels. Jabbr et al. [10] researched the performance of dual fuel engine. In order to figure out the influence rule of parameters and the balance of the state factors, they used the method of analysis of variance and genetic algorithm and neuron network. Results show that increasing the ratio of hydrogenated oil can reduce the soot generation and improve the performance of combustion. Allam et al. [11] studied the economic efficiency and air filter of the diesel engine. Zhang [12] studied the influence rule of boiling heat transfer on the performance of diesel engine. They verified the simulation results of boiling heat transfer and the general heat transfer. They also used the perturbation method to investigate parameters of diesel engine.

As for the high temperature in the engine, the researches focused on the cylinder liner [13], piston [14], cylinder head [15], cylinders [16], crank [17], shaft [18], and so on. Zhaoju et al. [19] studied the thermal-mechanical coupling stress of the piston. Based on the calculated results, they optimized the piston about its top height and its pin bore using the response surface method. Results show that the geometry of piston does not have obvious effect on the temperature and stress of the piston. At last, to decrease the maximum stress and mass of piston, they used the multiobjective optimization method to optimize the piston. Wang et al. [20] studied the fatigue rule of the piston alloy and come up with a life prediction method to evaluate the working state and left life of the piston. They studied the properties of piston among high and low temperature. Based on the model and the calculation results, they provided the optimal strategy to guarantee the reliability and working life of piston alloy. Wang et al. [21] researched the seal of cone using the method of finite element method. They established the model of cone combing with gasket, considering the effect of relaxation and long time working, and studied the leakage rule of the cone at the different conditions. This study can contribute to the reliability of satellite and its seal performance. Liu et al. [22] studied the experimental method to measure the heat transfer coefficient of refrigerator gasket. They used the reverse heat loss method to specify the heat flow through the gasket. To guarantee the experimental results, they used three gaskets and divided the heat transfer area small enough to measure the heat transfer condition. By experiment and analysis, they find some methods which could enhance the seal ability and could decrease the heat transfer coefficients. Rashnoo et al. [23] used two methods to optimize the alloy used in cylinder gasket, which is different displacement rates and reinforcement. To figure out the influence of these two factors, they used the method of sensitivity analysis and regression analysis. Results show that the reinforcement has more influence on the alloy strength and that the alloy microstructure will be better after the reinforcement.

The orthogonal experiment method is applied in the research widely; the related subject and issues are composite material [24], road construction [25], plasma spray [26], batteries [27], alloy powder [28], and concrete properties [29]. Subramani et al. [30] explored the method to improve the quality of exhaust and minimize the variation of performance of engine. They selected a single cylinder engine and its eight factors to perform the study. The target objective of the research is the quality of the exhaust and engine performance and the method used in this study are taguchi design, analysis of variance, and the response surface methodology. Nagasankar et al. [31] researched the welding process of the exhaust value of engine. They used the orthogonal experiment to investigate the influence rule of pressure, time, and other factors on the welding quality. Based on the calculation results, they conducted the multiple liner regression and variance analysis.

The applied fields of hybrid neural network are more and more wide with the development of the algorithm. The related research areas are stock market [32], language identification [33], property prediction [34], life prediction of component [35], emotion recognition [36], and so on. Baklacioglu et al. [37] used a new method to establish the mathematical model of engine; the method is hybrid genetic algorithm artificial neuron network strategy. In the calculation process, five state parameters of engine are set as input factors and the condition of the main components as output. Results show that the method has a good prediction accuracy. Jiang et al. [38] conducted the output prediction of the engine using artificial neuron network. They established two improved artificial neuron networks for two engines and used the extended database to train the model. Results show that two improved networks have more prediction accuracy than the original network and that the improved networks have better robustness when facing different datasets. Fagundez et al. [39] established the model of engine with the methods of artificial neuron network and particle swarm optimization artificial neuron network, respectively. Results show that both algorithms are applicable for the prediction of performance of engine. It can be concluded that the particle swarm optimization artificial neuron network method has more prediction accuracy in emissions compared to artificial neuron network. Chen et al. [40] studied the effectiveness of fault diagnosis using hybrid neuron network based on the extensive experiment data. During the process of training and diagnosis, they captured the feature

of data by method of convolutional and recurrent computing and trained the network by method of convolutional and recurrent backpropagation algorithm. Results show that the method is verified to do the diagnosis. Cui et al. [41] studied the predictive method of fuel saving on the washing engine; the method they used was singular value decomposition, convolutional neural network, and empirical mode decomposition. To improve the prediction accuracy, they replaced the continuous flight data by discrete data to train the model which would be used to predict the quantity of fuel savings.

There are many researches that focus on grey wolf optimization, which are related to grid [42], fuel cell [43], robot controlling [44], blend fuel [45], engines [46], forecasting of investment [47], and so on. Gujarathi et al. [46] optimized the engine with grey wolf algorithm for its performance and emissions. In the optimization process, a wide range of parameters are considered, including specific fuel consumption, hydrocarbon, carbon monoxide, nitrogen oxide, and particulate matters. Results show that grey wolf algorithm can find the optimal values with least costs. Ileri et al. [45] studied the optimization problem of cetane concentration in blend fuel used in diesel engine. They conducted a series of experiment under different conditions and using the grey wolf algorithm to find the optimal results of the blend. At the optimization process, they took the performance of engine and emission of combustion into consideration. At last they find the optimal fuel composition under different conditions and calculate the performance results. Luo et al. [48] come up with an improved grey wolf algorithm by improving the weight of leader wolf location. Considering the convergence speed and the optimization accuracy, the new algorithm is better than the original one. The new algorithm has a low cost when calculating the actual engineering problems. Vijay and Nanda [49] optimized the grey wolf algorithm with three strategies which are prey weight, control level, and both of them. They compared the new algorithm's performance with other five algorithms and the compared parameters are data scalability, noise, and algorithm parameter. Results show that the new algorithm has advantage in solving engineering problems.

The paper mainly optimizes the operating factors of cylinder gaskets based on their maximum temperature, maximum stress, and maximum deformation. The methods involved in the process mainly contain finite element method, orthogonal experimental design, a hybrid neural network model based on partial least squares regression and deep neural network, and grey wolf optimization algorithm based on an artificial bee colony algorithm. In different parts, the corresponding research contents are described below. In Part 1, FEM is utilized to figure out and analyze temperature fields, thermal-mechanical coupling stress fields, and deformations of cylinder gaskets and to analyze areas where operating conditions are comparatively poor. In Part 2, orthogonal experimental design method is adopted to calculate and analyze the influence rules of five operating factors (i.e., the diameter of the combustion chamber circle, the diameter of coolant channel, the length of thermal insulation area between the 3rd and 4th cylinders, the thickness of cylinder gasket, and bolt preload force) on three state parameters of the cylinder gaskets (i.e., the maximum temperature, maximum stress, and maximum deformation of the gasket), and the four operating factors which most significantly affect these state parameters are determined. In Part 3, a hybrid neutral network based on partial least squares regression and deep neural network is applied to establish the corresponding relationship between 4 operating factors and 3 state parameters. In Part 4, on the foundation of grey wolf algorithm, three different weight coefficients are introduced to weigh the locations of three kinds of grey wolves so as to figure out the preys' location in a more accurate way. In addition, artificial bee colony algorithm is also adopted to calculate three weight coefficients. In Part 5, the optimal operating factors of the gaskets can be determined by the calculation in combination with the hybrid neural network and the improved grey wolf algorithm.

1.1. Analysis of Cylinder Gasket Working Condition. As the most important sealing component in diesel engine [50], cylinder gaskets function with the primary goals of reliable combustor and coolant channel sealing by virtue of material elasticity. In practice, not only are cylinder gaskets subjected to bolt preload forces and scour from high-temperature and high-pressure gases inside the cylinder, but some areas in them exposed to the coolant may be corroded. In this consideration, cylinder gaskets should meet the following requirements [51]. With certain flexibility and elasticity, they are capable of compensating for roughness and deformation on the interface; with sufficient mechanical strength, they have the ability to support bolt preload forces and the subsidiary loads generated by interface deformation, and under actions of high-pressure gases, it is less likely for gasket to be damaged; with heat and corrosion resistance, they cannot be easily eroded by cooling liquid and no ablation takes under actions of high-temperature gases; at last, with convenient assembly and disassembly, they can be capable of recycling and have a long service life.

According to the proposed working process model of diesel engine and data achieved by experiments, boundary conditions are figured out for temperature fields and thermal-mechanical coupling stress fields of cylinder gaskets. As measured through experiment, bolt preload force of gaskets on the diesel engine turns out to be 153.8 kN. To calculate the temperature of gasket accurately, a coupling heat transfer model is established specific to high-temperature parts inside the diesel including cylinder head, cylinder gasket, cylinder body, and cylinder sleeve. In this manner, temperature field of the cylinder gasket is acquired.

Temperature fields of the cylinder gasket have been presented in Figure 1. To validate accuracy of these results, the real temperature of the cylinder gasket in engine is measured. Considering that the gasket is located between cylinder body and head, only its exterior area can be measured under the circumstance that the diesel engine is not dismantled. The location of measuring points is shown in Figure 2. Comparison between experimental values and

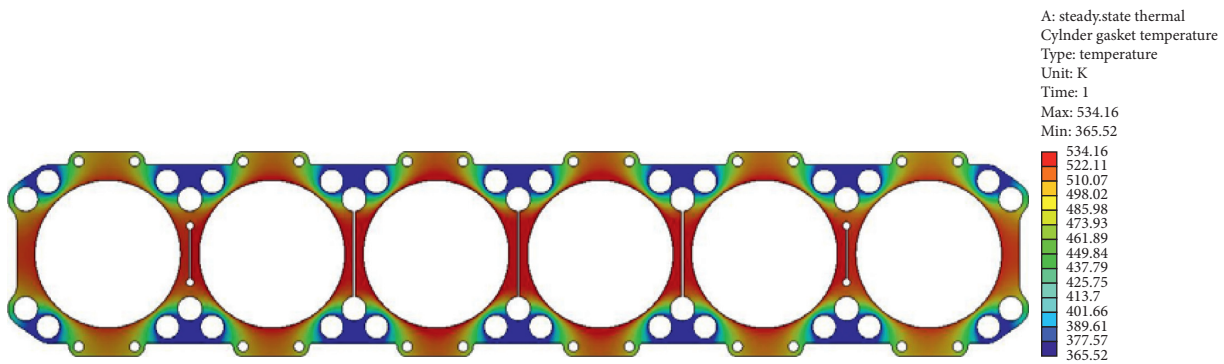

Figure 1: The results of gasket temperature field.

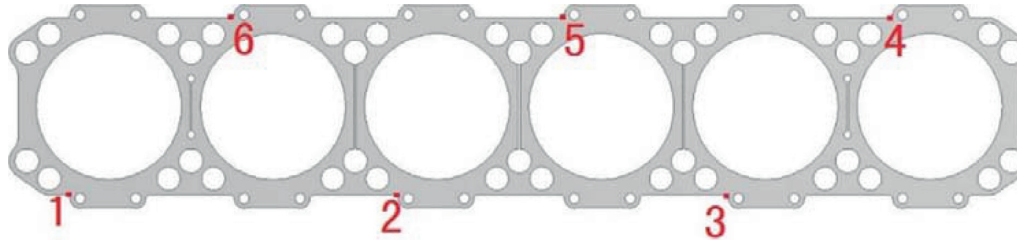

Figure 2: The schematic diagram of experimental measuring point arrangement for gasket temperature fields.

the calculated values is listed in Table 1. As can be observed from Table 1, the maximum error between the calculated value and the experimental value is 7.1%, which satisfies the accuracy requirement of engineering calculation.

As shown in Figure 1, maximum temperature (534.16 K) of the gasket is achieved at the middle position between the 3rd and the 4th cylinders, and such a position is in contact with the combustor. Moreover, the minimum temperature is 365.52 K, found nearby the coolant channel. Overall, cylinder gaskets with moderate temperature values are faced with a high-temperature gradient; with the conditions that materials are soft and flexible, great importance should be attached to their temperature and stress conditions.

The thermal-mechanical coupling stress field of the cylinder gasket at the moment of maximum explosion pressure of first cylinder is presented in Figure 3. Clearly, it is revealed by this figure that maximum thermal-mechanical coupling stress of the gasket is 246.17 MPa, found in the position next to the coolant channel of first cylinder. Besides the action of scour generated by the explosion pressure within the cylinder, such an area is also under the influence of heat transfer from high-temperature gas, heat dissipation to the coolant, and heavy mechanical and thermal loads. Therefore, its thermal-mechanical coupling stress is comparatively high. Additionally, this figure also reflects that the influence of the maximum explosion pressure on cylinder gaskets is only limited to areas close to the first cylinder. This signifies that bold preload force, together with interaction of cylinder body and head, plays a favorable role in fixing and supporting the cylinder gasket.

As for deformation of cylinder gasket, it is presented in Figure 4. Here, maximum deformation of the cylinder gasket is 0.3771 mm, which principally takes place in exterior areas of 1st and 6th cylinders. Moreover, the deformation is appeared to gradually increase from the center towards both sides of the gasket.

Through analysis on temperature fields, thermal-mechanical coupling stress fields, and the deformation condition of cylinder gaskets, it is found that thermal-mechanical coupling stress is rather high at the area near the coolant channel. In addition, deformation condition of both sides is still considerable. Considering that materials are soft, it is much likely for cylinder gaskets to suffer fatigue failure and damage. Hence, research on operating factors optimization is carried out in the following parts.

2. Analysis of Cylinder Gasket Operating Factors based on Orthogonal Experiment

2.1. Experimental Design. As can be known from the above analysis, coupling stress and deformations of cylinder gaskets are comparatively high in the process of their operation. For this reason, orthogonal experimental design was conducted to realize optimal design of such gaskets and further identify the optimal operating factors. It is shown by calculation result that gasket temperature reaches its maximum value in the area nearby the "combustion chamber circle," and the maximum stress is found in the area between the "combustion chamber circle" and the "coolant channel circle." The most serious condition of gasket occurred at the area between 3rd and 4th cylinders. In this context, the following five factors are selected to be optimized, including "radius of combustion chamber circle, A," "radius of coolant

Table 1: The comparison between experimental and calculated temperature values of the gasket.

Measuring points	1	2	3	4	5	6
Experimental values	414.73	417.59	412.711	420.054	417.4528	422.839
Calculated values	391.81	414.75	432.88	446.83	447.10	440.32
Errors (%)	5.53	0.68	−4.89	−6.37	−7.10	−4.13

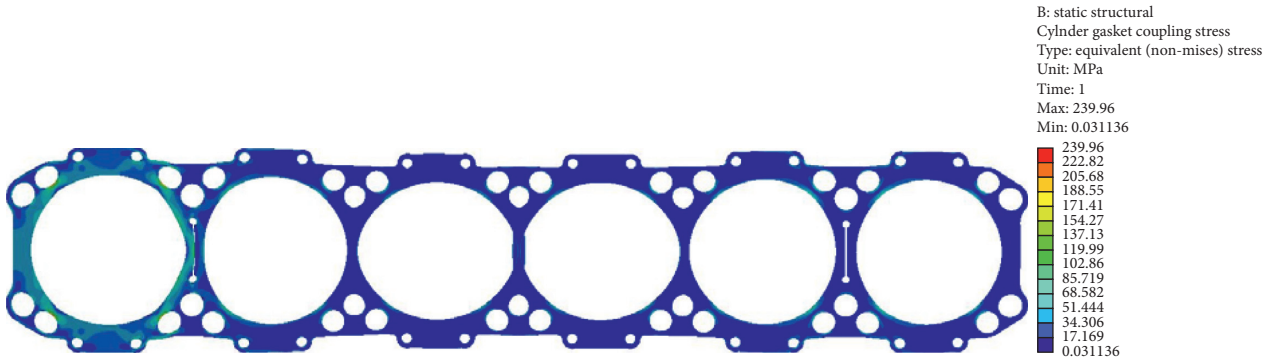

Figure 3: The schematic diagram of thermal-mechanical coupling stress distribution of cylinder gasket.

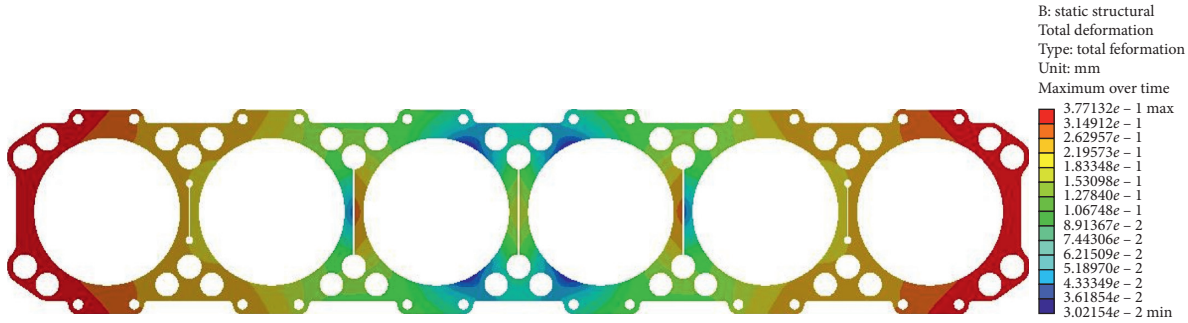

Figure 4: The schematic diagram of cylinder gasket deformations.

channel, B," "length of insulation area between 3rd and 4th cylinder, C," "thickness of cylinder gasket, D," and "bolt preload force, E."

The experiment is concerned with 5 levels in total, which means, for each factor, 5 values were selected for computational analysis. The corresponding levels of different factors are listed in Table 2. Here, the table of $L_{25}(5^6)$ was adopted to fulfill the experimental design. $L_{25}(5^6)$ means that this table totally consists of 25 experiments, 6 factors in each experiment and 5 values corresponding to each factor. For details, please refer to the left section of Table 3.

2.2. Statistical Analysis of Experimental Results. As orthogonal experimental design is performed for cylinder gaskets, corresponding maximum temperature T_{max}, maximum coupling stress S_{max}, and maximum deformation D_{max} of gasket were, respectively, figured out. The computing results have been listed in Table 3.

It is clear in Table 4 that the minimum value of T_{max} is 524.16 K, obtained from the experimental group 3, while

Table 2: The levels of different factors.

Factors	A	B	C	D	E
1	153	23	1	2	133.8
2	154	24	1.25	2.5	143.8
3	155	25	1.5	3	153.8
4	156	26	1.75	3.5	163.8
5	157	27	2	4	173.8

minimum values of S_{max} and D_{max}, respectively, 225.18 MPa and 0.2075 mm, are found in experimental groups 22 and 14, respectively. Additionally, relevant results should be further analyzed, which is shown in Table, because optimal values of three state parameters are acquired from different groups of experiments and it is impossible to evaluate influence rules of various factors merely dependent on their optimal values.

Tables 1 to 5 represent sums of state parameters' values corresponding to levels 1–5 of various factors; Max and Min stand for maximum and minimum values of 5 data in the corresponding columns, and R is the difference between

Table 3: The arrangement and computing results of experiment.

Number	A	B	C	D	E	F	T_{max}	S_{max}	D_{max}
1	1	1	1	1	1	1	536.24	243.51	0.4844
2	1	2	2	2	2	2	534.47	242.7	0.285
3	1	3	3	3	3	3	524.16	230.02	0.3095
4	1	4	4	4	4	4	534.99	237.63	0.3509
5	1	5	5	5	5	5	536.12	250.01	0.4496
6	2	1	2	3	4	5	531.18	253.76	0.3629
7	2	2	3	4	5	1	536.85	226.73	0.4253
8	2	3	4	5	1	2	533.37	251.56	0.4963
9	2	4	5	1	2	3	536.45	225.64	0.3836
10	2	5	1	2	3	4	535.8	229.66	0.3501
11	3	1	3	5	2	4	531.38	256.49	0.3825
12	3	2	4	1	3	5	533.18	233.61	0.3853
13	3	3	5	2	4	1	531.62	243.36	0.2488
14	3	4	1	3	5	2	531.3	235.74	0.2075
15	3	5	2	4	1	3	534.81	245.86	0.4761
16	4	1	4	2	5	3	536.38	247.56	0.3223
17	4	2	5	3	1	4	531.18	244.87	0.4411
18	4	3	1	4	2	5	535.67	247.27	0.3581
19	4	4	2	5	3	1	535.87	232.76	0.3543
20	4	5	3	1	4	2	533.99	242.24	0.3447
21	5	1	5	4	3	2	536.4	261.49	0.2194
22	5	2	1	5	4	3	532.73	225.18	0.2978
23	5	3	2	1	5	4	531.76	233.14	0.3444
24	5	4	3	2	1	5	532.71	238.26	0.3775
25	5	5	4	3	2	1	533.86	243.55	0.3265

Max and Min. "Tem," "Str," and "Def" are temperature, stress, and deformation of the gasket, respectively.

As observed from the table, factors A and D have great influence on deformations of gasket; coupling stress of gasket is dramatically affected by factor B, and temperature of gasket is under high influence of factor D. Considering that three parameters (i.e., temperature, stress, and deformation) are associated with factors A, B, and D, it is difficult to comprehensively confirm gasket's optimization conditions simply depending on the table. For this reason, experimental results are further analyzed by a variance analysis method.

2.3. Variance Analysis of Experimental Results. During variance analysis on experimental results, mathematical statistics method is used to be sure whether differences in experimental results are incurred by differences in levels corresponding to factors or by experimental errors [52]. In this way, influence of various factors on experimental results may be analyzed in a more intuitive manner.

Firstly, the sum of squares of deviations can be expressed in the following equation as far as various factors are concerned:

$$S_i^2 = \frac{\mathrm{I}_i^2 + \mathrm{II}_i^2 + \mathrm{III}_i^2 + \mathrm{IV}_i^2 + \mathrm{V}_i^2}{n_{sp}} - \frac{T^2}{n_z}. \quad (1)$$

In the above equation, i is the number of column and is equal to 1–5; n_{sp} is level repeat number and is 5 in this article; T and n_z, respectively, refer to summation and the total number of data, where $n_z = 25$. In this case, factors' degree of freedom that corresponds to the sum of squares of deviations can be written into the following equation:

$$f_i = n_{sp} - 1. \quad (2)$$

After sums of squares of deviations of all factors have been worked out, error sums of squares of experimental results can be obtained based on the following equation:

$$S_e^2 = S_T^2 - S_1^2 - S_2^2 - S_3^2 - S_4^2 - S_5^2. \quad (3)$$

In line with the following formula:

$$S_T^2 = \sum S_i^2. \quad (4)$$

The error sum of squares here can be expressed as follows:

$$S_e^2 = S_6^2. \quad (5)$$

Afterwards, mean square values are obtained in accordance with the following equation:

$$F_i = \frac{S_i^2/f_i}{S_e^2/f_e}. \quad (6)$$

If the critical value of F is close to 1, it indicates that influence of level variations on state parameters is similar to that of experimental errors on them. Therefore, it is deemed that this factor has no significant influences on state parameters. Otherwise, it is believed that the factors enormously affect state parameters. In this study, probability

Table 4: Further analysis of computing results.

Factor		I	II	III	IV	V	Max	Min	R
A	Temp	2665.98	2673.65	2662.29	2673.09	2667.46	2673.65	2662.29	11.36
	Str	1203.87	1187.35	1215.06	1214.7	1201.62	1215.06	1187.35	27.71
	Def	1.88	2.02	1.7	1.82	1.565	2.02	1.565	0.455
B	Temp	2671.58	2668.41	2656.58	2671.32	2674.58	2674.58	2656.58	18
	Str	1262.81	1173.09	1205.35	1170.03	1211.32	1262.81	1170.03	92.78
	Def	1.77	1.835	1.755	1.675	1.945	1.945	1.675	0.27
C	Temp	2671.74	2668.09	2659.09	2671.78	2671.77	2671.78	2659.09	12.69
	Str	1181.36	1208.22	1193.74	1213.91	1225.37	1225.37	1181.36	44.01
	Def	1.7	1.825	1.84	1.88	1.74	1.88	1.7	0.18
D	Temp	2671.62	2670.98	2651.68	2678.72	2669.47	2678.72	2651.68	27.04
	Str	1178.14	1201.54	1207.94	1218.98	1216	1218.98	1178.14	40.84
	Def	1.94	1.585	1.65	1.83	1.98	1.98	1.585	0.395
E	Temp	2668.31	2671.83	2665.41	2664.51	2672.41	2672.41	2664.51	7.9
	Str	1224.06	1215.65	1187.54	1201.79	1222.91	1224.06	1187.54	36.52
	Def	2.275	1.735	1.62	1.605	1.75	2.275	1.605	0.67

Table 5: The variance analysis of results.

State parameters	Factor	S_i^2	S_i^2/f_i	F value	Critical value of F			Significance
					0.10	0.05	0.01	
T_{max}	A	18.717	4.679	0.540	2.250	2.870	4.430	
	B	39.300	9.825	1.133	2.250	2.870	4.430	
	C	24.133	6.033	0.696	2.250	2.870	4.430	
	D	80.837	20.209	2.331	2.250	2.870	4.430	※
	E	10.376	2.594	0.299	2.250	2.870	4.430	
S_{max}	A	103.673	32.818	0.278	2.250	2.870	4.430	
	B	1124.412	126.088	3.018	2.250	2.870	4.430	※※
	C	237.836	42.609	0.638	2.250	2.870	4.430	
	D	211.473	42.408	0.568	2.250	2.870	4.430	
	E	185.625	67.386	0.498	2.250	2.870	4.430	
D_{max}	A	0.024	0.006	0.984	2.250	2.870	4.430	
	B	0.008	0.002	0.328	2.250	2.870	4.430	
	C	0.004	0.001	0.164	2.250	2.870	4.430	
	D	0.061	0.01525	1.025	2.250	2.870	4.430	
	E	0.12	0.03	2.500	2.250	2.870	4.430	※

distribution of factor F is selected to evaluate influence of factors on state parameters. The computing results are presented in Table 5.

It is embodied by analysis results in the table that temperature of cylinder gaskets suffers great influence of factor D (thickness of cylinder gasket), and the corresponding F value is 2.331. In terms of stress of cylinder gaskets, factor B (radius of coolant channel) has a tremendous influence on it and the corresponding F value reaches 3.018. As for the cylinder gasket deformation, it is under a significant influence of factor E (bolt preload force) and the F value in this case turns out to be 2.5. As proven by the results in Tables 4 and 5, three state parameters are considerably affected by factors A, B, D, and E. On this account, only the influence of such four factors on state parameters of cylinder gaskets is taken into consideration during subsequent computational analysis. The above calculations and analyzation can only obtain cylinder gasket optimization situations in several discrete and limited conditions. Based on these situations, we cannot optimize cylinder gaskets to find its optimal operating factors accurately. Therefore, an approach based on hybrid neural network is put forward so that the existing optimization research on cylinder gaskets can be extended from a limited point working condition to an unlimited surface working condition.

3. Operating State Prediction for Cylinder Gaskets Based on Hybrid Neural Network

Depending on the above analysis and calculations, an operating state prediction method is proposed for cylinder gaskets according to relatedness of 4 operating factors to be optimized and 3 state parameters of diesel cylinder gaskets, and the prediction method mainly based on partial least squares regression (PLSR) and Deep Neuron Network (DNN).

3.1. Hybrid Neural Network Based on PLSR and DNN.

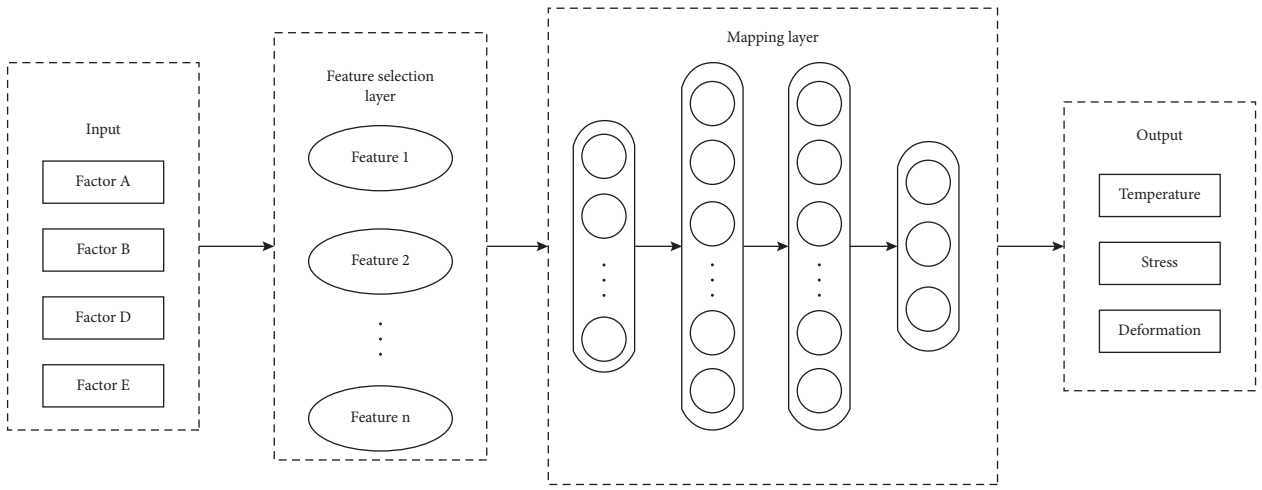

Figure 5: The main process of hybrid neutral network.

The neural network selected for this study is mainly divided into two layers. While one layer is known as a feature selection layer, the other layer is a mapping layer. In terms of the former, a PLSR algorithm [53] is utilized to perform feature selection for cylinder gasket operating factors to be optimized; as for the latter, a DNN [54] is used to establish mapping between features of operating factors to be optimized and state parameters of cylinder gaskets. Through joint actions of such two layers, an operating state prediction model is built for cylinder gaskets according to the hybrid neural network based on PLSR and DNN. Additionally, basic working process of the hybrid neural network based on PLSR and DNN is shown in Figure 5 [55].

Next, both the feature selection layer and the mapping layer are briefly described.

3.2. Feature Selection Layer. Four normalized operating factors, to be optimized, of the cylinder gasket are selected as input of the feature selection layer, and the purpose of regression is to acquire extrema of state parameters related to the cylinder gasket. Moreover, corresponding output result can be seen as linear approximation of state parameters [56]. Respectively, input parameters and output targets can be expressed as follows:

$$P_{\text{in}} = \left[p_1^{\text{T}}, p_2^{\text{T}}, \cdots, p_n^{\text{T}}\right], \tag{7}$$

$$G_{\text{out}} = \left[g_1^{\text{T}}, g_2^{\text{T}}, \cdots, g_m^{\text{T}}\right], \tag{8}$$

where P_{in} stands for the input data matrix, G_{out} for a feature selection data matrix, p_1^{T} for input sample vectors, and g_1^{T} for a matrix of selected features.

Using these two equations to do the space projection of the previous two data matrixes,

$$P_{\text{in}}\omega_1 = p_1\omega_{11} + p_2\omega_{12} + \cdots + p_n\omega_{1n} = t_1, \tag{9}$$

$$G_{\text{out}}\upsilon_1 = g_1\upsilon_{11} + g_2\upsilon_{12} + \cdots g_m\upsilon_{1m} = u_1, \tag{10}$$

where ω_1 is eigenvector of $P_{\text{in}}^{\text{T}}G_{\text{out}}G_{\text{out}}^{\text{T}}P_{\text{in}}$ and υ_1 represents eigenvector of $G_{\text{out}}^{\text{T}}P_{\text{in}}P_{\text{in}}^{\text{T}}G_{\text{out}}$.

Here, correlation of t_1 and u_1 is primarily investigated. Once the spatial correlation reaches its maximum level, a regression model is established as follows:

$$P_{\text{in}} = t_1\alpha_1 + E_1, \tag{11}$$

$$G_{\text{out}} = t_1\beta_1 + F_1, \tag{12}$$

where α_1 and β_1 are parameter vectors and E_1 and F_1 are residuals matrixes.

Furthermore, the following formulas can be acquired:

$$P_{\text{in}} = t_1\alpha_1 + t_2\alpha_2 + \cdots + t_r\alpha_r + E_r, \tag{13}$$

$$G_{\text{out}} = t_1\beta_1 + t_2\beta_2 + \cdots + t_r\beta_r + F_r, \tag{14}$$

$$\alpha_i = \frac{P_{\text{in}}^{\text{T}}t_i}{t_i^2}, \tag{15}$$

$$\beta_i = \frac{G_{\text{out}}^{\text{T}}t_i}{t_i^2}, \tag{16}$$

$$t_i = P_{\text{in}}\omega_i, \tag{17}$$

where r represents a rank of matrix P_{in} and both E_r and F_r are least-residuals matrixes.

By combining the above formulas simultaneously, the PLSR equation is achieved as follows:

$$G_{\text{out}} = P_{in}\omega_1\beta_1 + P_{in}\omega_2\beta_2 + \cdots + P_{in}\omega_r\beta_r + F_r. \tag{18}$$

By virtue of the above equation, dimensionality reduction and feature selection can be fulfilled for data at the minimum cost (i.e., the least residuals).

3.3. Mapping Layer. Here, output of the feature selection layer acts as the input of the mapping layer. Through the

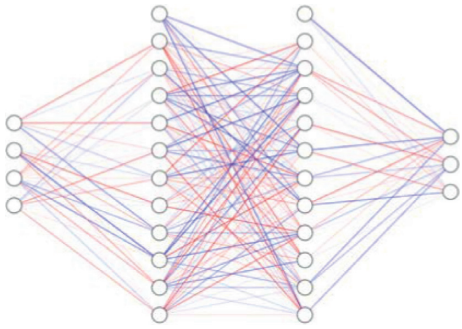

Figure 6: DNN framework.

weighting operation which is based on DNN containing two hidden layers, the data is eventually mapped on three state parameters of cylinder gaskets. The core of the mapping layer is DNN which includes the multihidden layer. Comparing with other mapping structures, DNN is capable of adapting to the nonlinear mapping process more accurately [57].

The proposed DNN framework is shown in Figure 6.

In the figure above, the output matrix of the first hidden layer is expressed as follows:

$$a_1 = g_1\left(W_1^{\mathrm{T}} x + b_1\right). \tag{19}$$

The output matrix of the second hidden layer is expressed in another equation:

$$a_2 = g_2\left(W_2^{\mathrm{T}} a_1 + b_2\right). \tag{20}$$

The matrix of output values is denoted by the following equation:

$$\widehat{y} = g_0\left(W_3^{\mathrm{T}} a_2 + b_3\right). \tag{21}$$

In the previous equation, $g_1(X)$, , $g_2(X)$ and $g_0(X)$ are activation functions; W_1, W_2, and W_3 are corresponding weight matrixes; and, b_1, b_2, and b_3 represent deviation matrixes.

When training using DNN, a loss function is introduced to evaluate training effects so that optimal weight matrixes and deviation matrixes can be achieved. For the purpose of avoiding overfitting, regularization is performed for the loss function. In this way, the final loss function can be written into the following equation:

$$J(W, b) = \frac{1}{m} \sum_{i=1}^{m} \left(\widehat{y}^i - y^i\right)^2 + \frac{\lambda}{2m} \sum_{j=1}^{n} W^{\mathrm{T}} W. \tag{22}$$

In this equation, m refers to the number of sample sets, $\widehat{y}^i$ to predicted values of data in group i, y^i to calculated values of data in group i, and λ to regularization parameters.

3.4. The Processing of Training Samples. Correspondence of state parameters and operating factors was figured out. Totally, 241 sets of data were obtained, among which 226 sets (group A) serve as training samples to train the PLSR and DNN based hybrid neural network model. As for the remaining 15 sets (group B), they were used to check the neural network. Some of these training samples are presented in Table 6.

Table 6: Part of training samples for hybrid neural network.

Number	A	B	D	E	$T_{\max}$	$S_{\max}$	$D_{\max}$
1	153	23.1	2.05	134.8	532.3381	241.4961	0.46534
2	153	24.2	2.6	145.8	534.0272	240.6686	0.28951
3	153	25.5	3.25	158.8	529.6143	235.9869	0.329427
4	153	26.8	3.9	171.8	532.3895	246.3937	0.427519
5	154	23.1	3.05	164.8	528.7039	252.5735	0.366654
6	154	24.4	3.7	157.8	530.7526	238.5101	0.454281
7	154	25.7	2.6	140.8	530.554	235.3738	0.416173
8	154	27	2.5	153.8	535.8	229.66	0.3501
9	155	23.3	3.4	146.8	534.3776	251.1415	0.383875
10	155	24.6	2.3	159.8	534.8501	238.6299	0.302998
11	155	25.9	2.95	172.8	533.9187	237.7446	0.210332
12	155.2	26.2	3.3	141.8	532.5061	248.4274	0.44481
13	156	23.5	2.75	153.8	537.0808	244.8637	0.385204
14	156	24.8	3.4	141.8	536.8542	248.0838	0.371042
15	156	26.1	3.8	154.8	534.3468	232.0513	0.353681
16	156.4	25.4	2.6	159.8	530.9911	247.8942	0.291781
17	157	23.7	3.85	160.8	535.0463	237.8009	0.272666
18	157	25	2	173.8	531.76	233.14	0.3444
19	157	26.3	2.65	136.8	529.1457	242.2156	0.364453
20	157	27	3	143.8	533.86	243.55	0.3265

To prevent data differences from affecting training results, the following equation was utilized to normalize samples before training.

$$x_l = \frac{|x - x_{\min}|}{x_{\max} - x_{\min}}. \tag{23}$$

In the above equation, x_l refers to the processed data, x to raw data, x_m to the mean value of data, and $x_{\max}$ and $x_{\min}$ to maximum and minimum values of data, respectively.

3.5. Validation of Training Results. Data of group B were adopted to check prediction results which were generated from the model of hybrid neural network based on PLSR and DNN. Comparison between calculated and predicted values is shown in Table 7.

As revealed from the table, all errors between the predicted and the calculated values are within 4.72%, which satisfies engineering calculation requirements. Therefore, this hybrid neural network is applicable to subsequent calculations and analysis.

Next, this article will use this neural network to search the operating factors corresponding optimal state parameters combined with a new algorithm named artificial bee colony based grey wolf optimizer (ABC and GWO).

4. ABC and GWO Algorithm

On account of the above analysis, a grey wolf optimization (GWO) algorithm [58] was put forward based on artificial bee colony (ABC) method [59] so as to perform computational analysis on optimal operating factors. The proposed algorithm aims to locate prey locations (optimal solutions)

Table 7: The comparison between calculated and predicted values.

Num	T_{max}			S_{max}			D_{max}		
	Cal	Pre	Error (%)	Cal	Pre	Error (%)	Cal	Pre	Error (%)
1	534.47	518.88	2.92	242.70	244.30	−0.66	0.28500	0.28448	0.18
2	530.30	549.12	−3.55	230.07	238.88	−3.83	0.30835	0.30637	0.64
3	527.60	515.45	2.30	234.42	228.21	2.65	0.34017	0.34077	−0.18
4	536.12	550.72	−2.72	250.01	251.31	−0.52	0.44960	0.46605	−3.66
5	534.01	529.07	0.92	252.55	264.47	−4.72	0.41185	0.41937	−1.83
6	537.03	528.73	1.54	224.76	233.98	−4.10	0.37450	0.36216	3.29
7	537.19	529.54	1.42	231.43	230.75	0.29	0.35352	0.36466	−3.15
8	533.76	548.69	−2.80	256.38	266.05	−3.77	0.38435	0.40143	−4.44
9	534.85	513.51	3.99	238.63	227.39	4.71	0.30300	0.30813	−1.69
10	533.26	517.57	2.94	248.15	247.10	0.42	0.38401	0.40146	−4.55
11	539.84	536.30	0.66	248.46	259.93	−4.62	0.35915	0.37588	−4.66
12	537.53	536.07	0.27	237.79	228.44	3.93	0.34507	0.34217	0.84
13	537.21	519.08	3.37	232.47	229.89	1.11	0.28220	0.27699	1.85
14	536.81	528.71	1.51	230.70	221.02	4.19	0.33111	0.32097	3.06
15	528.34	509.59	3.55	237.52	240.49	−1.25	0.37087	0.36707	1.02

by combining GWO with ABC. Here, this algorithm is named ABC and GWO.

4.1. Grey Wolf Optimization Algorithm. Grey wolf is a kind of social predators. Based on its methods of surrounding, attacking, and hunting, Mirjalili raised GWO algorithm. According to different command hierarchies, grey wolves are divided into three major categories by the algorithm. In line with hierarchical levels, such three categories are α wolf, β wolf, and δ wolf. Among them, grey wolves in the middle hierarchy are primarily in charge of assisting grey wolves at higher levels and directing grey wolves at lower levels [60].

During calculation, the population size of grey wolves is denoted as N, the search space is set to be d-dimensional, spatial position of grey wolf i is designed as $X_i = (x_1, x_2, \cdots, x_d)$, and spatial position of preys is set as $X_l = (x_1^*, x_2^*, \cdots, x_d^*)$. Moreover, the spatial position of preys is where grey wolves get together for hunting and it is also a global optimal solution of GWO.

In the process of hunting, position of grey wolves is updated by the following equations:

$$X(t+1) = X_l(t) - A * \left|C * X_l(t) - X(t)\right|, \tag{24}$$

$$A = 2(r_1 - E) * a, \tag{25}$$

$$C = 2r_2 * a, \tag{26}$$

where both r_1 and r_2 are random vectors, E refers to column vectors with all elements equal to 1, and a represents a convergence factor vector. As for the relational expression of a and E, it can be written as follows:

$$a = 2\left(\frac{(1-t)}{t_{max}}\right) * E^{T}. \tag{27}$$

For the convenience of subsequent representation, $|C * X_l(t) - X(t)|$ is denoted by D. Regarding wolves α, β and δ, their positions can be updated according to the following equations:

$$X_1 = X_\alpha - A_1 * D_\alpha, \tag{28}$$

$$D_\alpha = \left|C_1 * X_\alpha - X\right|, \tag{29}$$

$$X_2 = X_\beta - A_2 * D_\beta, \tag{30}$$

$$D_\beta = \left|C_2 * X_\beta - X\right|, \tag{31}$$

$$X_3 = X_\delta - A_3 * D_\delta, \tag{32}$$

$$D_\delta = \left|C_3 * X_\delta - X\right|, \tag{33}$$

where X_1, X_2, and X_3 are the latest positions of α, β and δ wolves after present iterative computations. In this case, position of preys can be figured out by the following formula:

$$X(t+1) = \frac{X_1 + X_2 + X_3}{3}. \tag{34}$$

GWO has the capability to sufficiently utilize information of wolves α, β and δ to carry out global search of optimal solutions. In this way, occurrence of local optimal solutions can be avoided to the greatest extent. However, influence of different types of wolves on optimal solutions is left out of consideration. Consequently, it is likely for excessive iterations or overfitting to take place. On this basis, a modified GWO based on ABC is proposed to calculate and analyze optimal operating factors of cylinder gaskets.

4.2. Calculation of Prey Positions. Considering that GWO fails to consider the influence of wolves α, β, and δ on prey positions, weight coefficients were introduced for such wolves in order to solve this defect; on this basis, the prey position can be figured out.

The modified prey position calculation formula is given in the following:

$$\widehat{X(t)} = \frac{\eta_1 X_1 + \eta_2 X_2 + \eta_3 X_3}{3}. \quad (35)$$

In the previous equation, η_1, η_2, and η_3 represent the weight coefficients related to three types of grey wolves.

The operating factors that correspond to optimal conditions of three state parameters of cylinder gaskets were obtained based on the results of orthogonal experiment. In specific calculation procedures, these operating factors were included into an optimal dataset DS; subsequently, data in DS were adopted to solve values of η_1, η_2, and η_3. After that, data in DS were updated in conformity with these values and corresponding cyclical iteration does not stop until data in DS remain unchanged.

During cyclical iteration described above, ABC was utilized to optimize values of η_1, η_2, and η_3. In the ABC algorithm, a bee colony is randomly produced using the equation

$$x_{ij} = x_j^{\min} + R^*\left(x_j^{\max} - x_j^{\min}\right), \quad (36)$$

$$R^* = \text{rand}\,(0, 1), \quad (37)$$

where x_{ij} represents ith bee in the bee colony, j is the number of solutions to the optimized problems, and $x_j^{\max}$ and $x_j^{\min}$ are maximum and minimum extrema of the optimization range.

The bee colony begins to look for nectar sources:

$$v_{ij} = x_{ij} + R^*\left(x_{ij} - x_{kj}\right), \quad (38)$$

where v_{ij} is a new nectar source (a new solution) nearby the current nectar source and x_{ij} and x_{kj}, respectively, stand for the current solution and a random solution next to the current solution. Once quality of the new nectar source is higher than that of the previous nectar source, the former can be reserved. In the entire process, an observing bee may identify where a new nectar source is at a certain probability according to quality of nectar sources. In order to figure out such a probability, the following equation should be followed:

$$P = \frac{\text{fit}_i\left(v_{ij}\right)}{\sum_{n=1}^{N} \text{fit}_n\left(v_{ij}\right)}, \quad (39)$$

where fit_i is a fitness function corresponding to a position of the ith nectar source.

4.3. Fitness Function. During practical calculations, a fitness function for the above ABCBGWO algorithm is defined as follows:

$$\text{fit}_i\left(v_{ij}\right) = \left(T_\alpha\widetilde{\left(v_{ij}\right)}\right)^2 + \left(S_\alpha\widetilde{\left(v_{ij}\right)}\right)^2 + \left(D_\alpha\widetilde{\left(v_{ij}\right)}\right)^2. \quad (40)$$

In the previous equation, α represents serial numbers of arrays for η_1, η_2, and η_3; $T_\alpha\widetilde{(v_{ij})}$, $S_\alpha\widetilde{(v_{ij})}$, and $D_\alpha\widetilde{(v_{ij})}$, respectively, refer to normalized temperature, stress, and deformations of cylinder gaskets under the circumstance that α set data are taken from η_1, η_2, and η_3.

4.4. The Main Procedure of ABC and GWO Algorithm. In essence, the ABC and GWO algorithm is a process during which three corresponding weight coefficients are introduced when prey positions are working based on wolves α, β and δ of the GWO, and then such three coefficients are further optimized by means of ABC. To be specific, major steps of this algorithm are described as follows.

Step 1: control variables of the grey wolf population are initialized, including the population size, the number of iterations, and the convergence factor vector.

Step 2: grey wolves are randomly generated, and the number of which is N. They are used to figure out prey positions which correspond to wolves α, β and δ.

Step 3: the number of iterations is set as $t = 1$ and iteration starts.

Step 4: the convergence factor vector a is updated.

Step 5: parameters of ABC are initialized, and the initial nectar source is randomly generated.

Step 6: the bee is directed to search for a new nectar source, and if the nectar source is better than all of the others, its position should be labelled as a potential one.

Step 7: the onlooker bee searches for and changes the labelled nectar source.

Step 8: a scout bee is determined to be present or not; if not, skip to Step 10.

Step 9: a new position is generated by the scout bee and replaces the current nectar source; in this case, the labelled nectar is changed.

Step 10: it is judged whether termination conditions are satisfied; if not, skip to Step 7.

Step 11: position of the grey wolf is updated and prey position is obtained by the combination of coefficients and grey wolf position.

Step 12: the value of the fitness function is figured out in this scenario.

Step 13: it is judged whether to continue the algorithm or not; if yes, please go back to Step 3.

Step 14: iteration is terminated and relevant results are output.

In this process, ABC is utilized in Steps 5–10 to calculate and analyze three weight coefficients; as for other steps, they represent an iteration framework of GWA.

Figure 7 presents a flow chart of the ABC and GWO algorithm.

5. Multiobjective Optimization of Cylinder Gasket Parameters

5.1. The Main Process. Regarding maximum temperature, maximum stress, and maximum deformation of the cylinder gasket, their least values are set as objects of multiobjective optimization. As far as the proposed algorithm is concerned, that described above is embodied in searching for the minimum value of the corresponding fitness function. As for

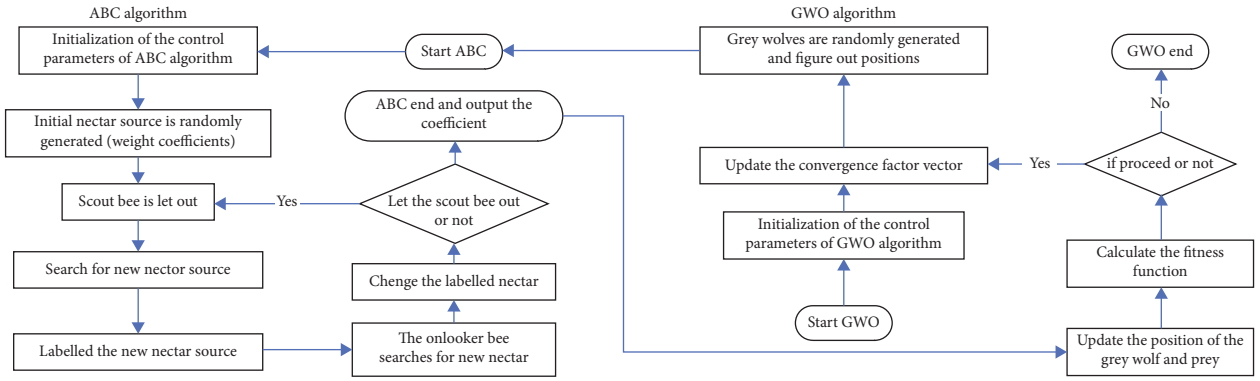

Figure 7: The flow chart of ABC and GWO algorithm.

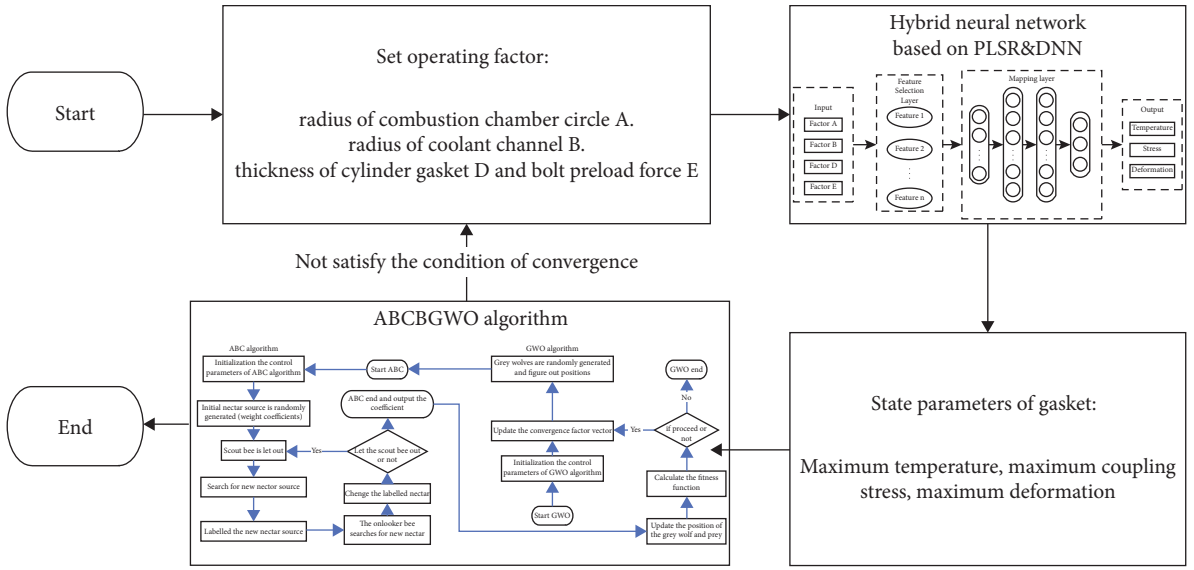

Figure 8: The main process of optimization.

Table 8: Initial values of different factors selected for multiobjective optimization.

Factors	A	B	C	D	E
Initial values	154	24	1.75	2.5	143.8

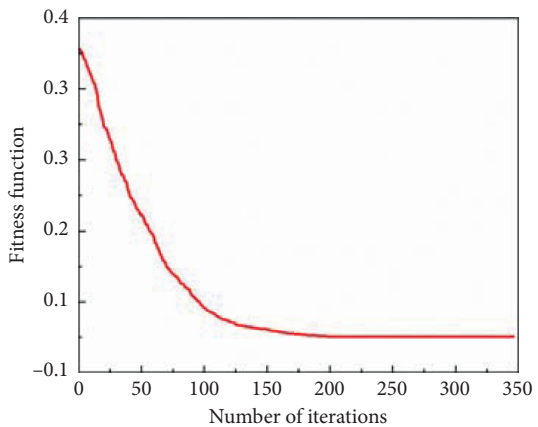

Figure 9: Variation rules of fitness function values.

Table 9: The RMSE and NRMSE of different algorithms.

	RMSE		NRMSE	
	Training	Evaluation	Training	Evaluation
HNN and ABCBGWO	2.5134	2.3674	0.0720	0.0740
Genetic algorithm	5.5476	5.7400	0.1578	0.1795
Support vector machine	3.4239	4.2288	0.0977	0.1322

Table 10: Optimal factors of cylinder gaskets calculated from the optimization algorithm.

Factors	A	B	C	D	E
Initial values	155	25	1.5	3	153.8
Optimal values	154	24.2	1.75	2.53	144.2

three state parameters of the cylinder gaskets, they are optimized in line with hybrid neural network based on PLSR and DNN as well as the ABC and GWO algorithm. Major procedures of the algorithm have been shown in Figure 8.

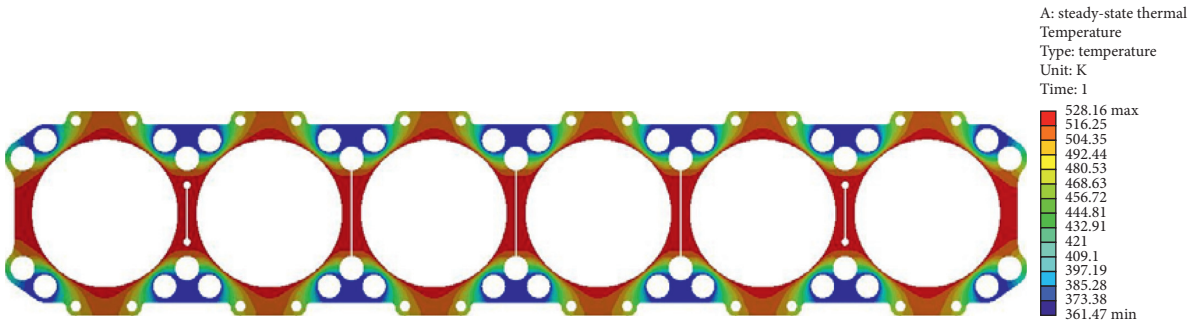

Figure 10: The schematic diagram of temperature field distribution of cylinder gaskets after optimization.

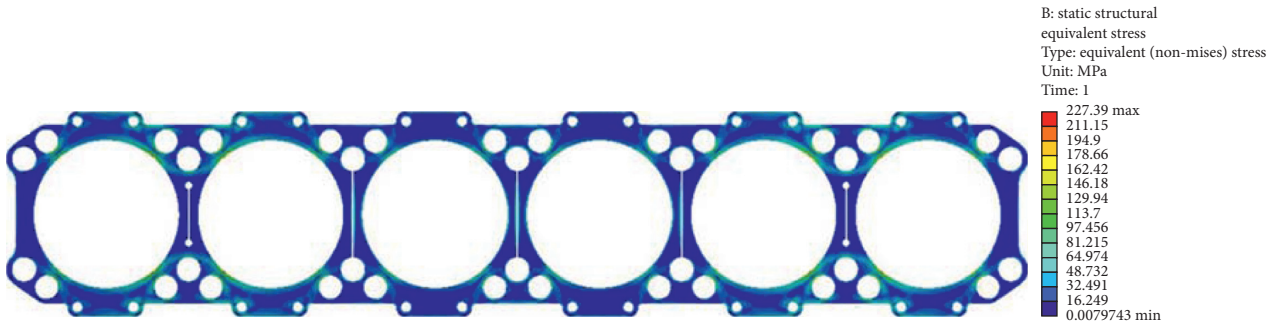

Figure 11: The schematic diagram of thermal-mechanical coupling stress field of gaskets after optimization.

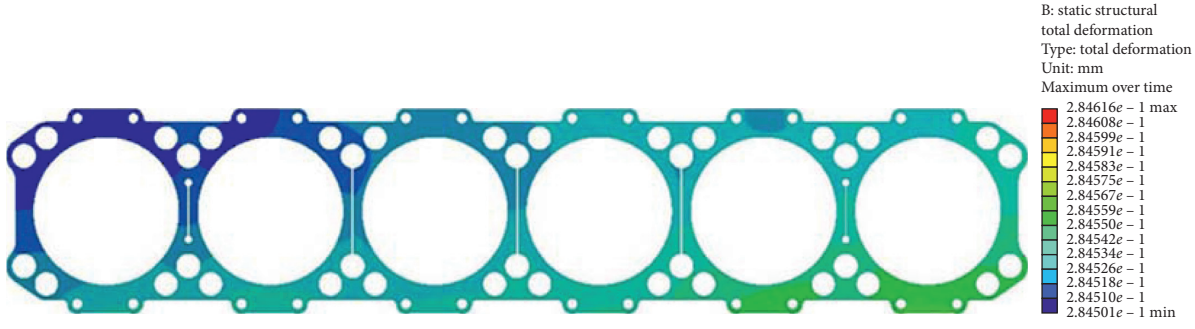

Figure 12: The schematic diagram of cylinder gasket deformation after optimization.

Table 11: The state parameters comparison before and after optimization.

Parameters	$T_{max}(K)$	S_{max} (MPa)	D_{max} (mm)
Before optimization	534.16	239.96	0.3771
After optimization	528.16	227.39	0.2846
Difference	6	12.57	0.0925
Percent of difference	1.12%	5.23%	24.52%

5.2. The Computing Process. Depending on Figure 8, three operating factors of the cylinder gaskets were optimized. Then, initial values of operating factors were eventually confirmed based on results of the orthogonal experiment; see Table 8.

In the course of calculation, values of the fitness function vary as the number of iterations changes. Corresponding variation rules have been shown in Figure 9.

To validate the performance of the hybrid neural network and ABCBGWO algorithm, the genetic algorithm and support vector machine are adopted to compare the RMSE and NRMSE of the predicted data with our algorithm. The detailed results are shown in Table 9.

From Table 9, we can conclude that, compared with genetic algorithm and support vector machine, the hybrid neural network and ABCBGWO can perform better in RMSE and NRMSE which proves the performance of the algorithm. In the next section, accuracy and effectiveness of the algorithm are examined.

5.3. Computing Results. In the light of hybrid neural network based on PLSR and DNN and the ABCBGWO algorithm, the optimal operating factors are figured out for diesel cylinder gaskets (as shown in Table 10).

Cylinder gasket is optimized using the values in Table 9. Afterwards, corresponding boundary conditions are utilized to establish FEM model of the gasket. Through computing, results of temperature fields, thermal-mechanical coupling stress fields, and deformations of the cylinder gasket are worked out, as shown in Figures 10–12.

Additionally, maximum temperatures, maximum thermal-mechanical coupling stresses, and maximum deformation of cylinder gaskets subsequent and prior to optimization are compared in Table 11.

Through the calculation results we can conclude that the maximum temperature, maximum coupling stress, and the maximum deformation of gasket are improved obviously. The maximum temperature, maximum coupling stress, and the maximum deformation decrease 6 K, 12.57 MPa, and 0.0925 mm compared to the original values, respectively. The thermal stress load and the deformation are relieved after the optimization, which proved the effectiveness of the algorithm.

6. Conclusion

The paper applies FEM, orthogonal experimental design, HNN, and GWO to optimize the operating factors in conjunction with state parameters of cylinder gaskets. The main tasks are described as follows:

(1) The FEM model is adopted to perform computational analysis on temperature fields, thermal-mechanical coupling stress fields, and deformations of cylinder gaskets; temperature field experiment is also conducted to validate accuracy of the computing model, and areas with comparatively high temperature and stress as well as obvious deformations are analyzed in line with computing results.

(2) Orthogonal experimental design is selected to investigate and analyze how operating factors of cylinder gaskets affect state parameters. Totally, there are 5 operating factors and 3 state parameters. In detail, the former includes the radius of combustion chamber circle, radius of coolant channel, length of insulation area between 3rd and 4th cylinder, thickness of cylinder gasket, and bolt preload force, while the latter consists of maximum temperature, maximum stress, and maximum deformation of the cylinder gasket. It is found that temperature, stress, and deformation of cylinder gaskets are under significant influences of the radius of combustion chamber circle, radius of coolant channel, thickness of cylinder gasket, and the bolt preload force. For this reason, subsequent analysis is made only specific to such four operating parameters.

(3) In order to overcome the problem of correspondence discontinuity between operating factors and state parameters of the cylinder gasket, a method is proposed to predict such a relation by virtue of a hybrid neural network model. To be specific, the hybrid neural network model consists of two layers in total. On the first layer, features of 4 operating factors are selected based on PLSR, and, on the second layer, the correspondence of feature of operating factors and state parameters is established according to DNN. As demonstrated by validation results, such prediction model of hybrid neural network is provided with accuracy that is high enough to meet engineering calculation requirements.

(4) When GWO is adopted to identify the prey's positions, differences in different grey wolves are neglected. With the goal of settling such a defect, three weight coefficients corresponding to three kinds of grey wolves are introduced to figure out prey positions, and ABC is also used to calculate and analyze values of such three weight coefficients. Not only is the defect of traditional GWA overcome, but final result can be obtained through rapid and accurate calculations by the proposed method. That is, such a method gives consideration to both computational efficiency and computing result accuracy.

(5) Orthogonal experimental design results, the proposed "the hybrid neural network model based on PLSR and DNN," and "ABCBGWO algorithm" are applied to figure out values of operating factors in the case where optimal state parameters are achieved for the cylinder gasket. Furthermore, operating factors of the cylinder gasket are optimized by virtue of computing results. Besides, the FEM model is utilized again to calculate and analyze corresponding temperature, stress, and deformations of the optimized gasket. It is revealed by results that state parameters of the optimized cylinder gasket are all improved, which proves good optimization effects and validity of the proposed algorithm.

Next, optimized cylinder gaskets will be subjected to experimental verification, and the proposed algorithm will be applied in optimization research on other high-temperature components inside the diesel cylinder. With respect to load reduction and reliability/service life improvement for high-temperature components and even the complete machine, such a study is of great significance.

Data Availability

The raw/processed data required to reproduce these findings can be accessed through the table in the article.

Conflicts of Interest

The authors declare that there are no conflicts of interest regarding the publication of this paper.

Acknowledgments

The research has received no fund by any institute or person.

References

[1] D. Khatri and R. Goyal, "Performance, emission and combustion characteristics of water diesel emulsified fuel for diesel engine: a review," *Materials Today: Proceedings*, vol. 28, no. 4, pp. 2275–2278, 2020.

[2] S. Uslu and M. Aydın, "Effect of operating parameters on performance and emissions of a diesel engine fueled with ternary blends of palm oil biodiesel/diethyl ether/diesel by Taguchi method," *Fuel*, vol. 275, Article ID 117978, 2020.

[3] S. Gopinath, P. K. Devan, C. Mohan, L. R. Krishna rao, P. Lokesh kumar, and S. Vara Prasad, "A review on influence of injection timing and injection pressure on DI diesel engine fuelled with low viscous fuel," *Materials Today: Proceedings*, In press, 2020.

[4] X. Xu, Z. Zhao, X. Xu et al., "Machine learning-based wear fault diagnosis for marine diesel engine by fusing multiple data-driven models," *Knowledge-Based Systems*, vol. 190, Article ID 105324, 2020.

[5] H. Sevinc and H. Hazar, "Investigation of performance and exhaust emissions of a chromium oxide coated diesel engine fueled with dibutyl maleate mixtures by experimental and ANN technique," *Fuel*, vol. 278, Article ID 118338, 2020.

[6] J. Jannatkhah, B. Najafi, and H. Ghaebi, "Energy and exergy analysis of combined ORC–ERC system for biodiesel-fed diesel engine waste heat recovery," *Energy Conversion and Management*, vol. 209, Article ID 112658, 2020.

[7] V. Kumar, A. P. Singh, and A. K. Agarwal, "Gaseous emissions (regulated and unregulated) and particulate characteristics of a medium-duty CRDI transportation diesel engine fueled with diesel-alcohol blends," *Fuel*, vol. 278, Article ID 118269, 2020.

[8] J. Wei, W. Lu, M. Pan, Y. Liu, X. Cheng, and C. Wang, "Physical properties of exhaust soot from dimethyl carbonate-diesel blends: characterizations and impact on soot oxidation behavior," *Fuel*, vol. 279, Article ID 118441, 2020.

[9] M. Subramaniam, J. M. Solomon, V. Nadanakumar, S. Anaimuthu, and R. Sathyamurthy, "Experimental investigation on performance, combustion and emission characteristics of DI diesel engine using algae as a biodiesel," *Energy Reports*, vol. 6, pp. 1382–1392, 2020.

[10] A. I. Jabbr, H. Gaja, and U. O. Koylu, "Multi-objective optimization of operating parameters for a H2/Diesel dual-fuel compression-ignition engine," *International Journal of Hydrogen Energy*, vol. 45, no. 38, pp. 19965–19975, 2020.

[11] S. Allam and A. M. Elsaid, "Parametric study on vehicle fuel economy and optimization criteria of the pleated air filter designs to improve the performance of an I.C diesel engine: experimental and CFD approaches," *Separation and Purification Technology*, vol. 241, Article ID 116680, 2020.

[12] Z. Zhang, J. E, J. Chen et al., "Effects of boiling heat transfer on the performance enhancement of a medium speed diesel engine fueled with diesel and rapeseed methyl ester," *Applied Thermal Engineering*, vol. 169, Article ID 114984, 2020.

[13] X. Peiyou, G. Daojing, H. Guannan et al., "Influence of piston pin hole offset on cavity erosion of diesel engine cylinder liner," *Engineering Failure Analysis*, vol. 103, pp. 217–225, 2019.

[14] E. Mancaruso and L. Sequino, "Measurements and modeling of piston temperature in a research compression ignition engine during transient conditions," *Results in Engineering*, vol. 2, Article ID 100007, 2019.

[15] E. Natesan, S. Eriksson, J. Ahlström, and C. Persson, "Effect of temperature on deformation and fatigue behaviour of A356–T7 cast aluminium alloys used in high specific power IC engine cylinder heads," *Materials*, vol. 13, no. 5, 2020.

[16] A. E. Segall, C. C. Schoof, and D. E. Yastishock, "Thermal solutions for a plate with an arbitrary temperature transient on one surface and convection on the other: direct and inverse formulations," *Journal of Pressure Vessel Technology Transactions of the ASME*, vol. 142, no. 5, 2020.

[17] M. Kota, N. Kyotaro, T. Yuichiro, and U. Kenko, "Control device for compression ignition type engine, and cylinder temperature determining method," US Patent-9719441B2, 2020.

[18] N. P. Starostin and M. A. Vasileva, "Determination of load-speed modes for fluoroplastic seals of rotary shaft by temperature limitation," vol. 459, 2020.

[19] Q. Zhaoju, L. Yingsong, Y. Zhenzhong, D. Junfa, and W. Lijun, "Diesel engine piston thermo-mechanical coupling simulation and multidisciplinary design optimization," *Case Studies in Thermal Engineering*, vol. 15, Article ID 100527, 2019.

[20] M. Wang, J. C. Pang, H. Q. Liu, S. X. Li, and Z. F. Zhang, "Property optimization of low-cycle fatigue in Al-Si piston alloy at elevated temperatures by ultrasonic melt treatment," *Journal of Materials Research and Technology*, vol. 8, no. 5, pp. 4556–4568, 2019.

[21] L.-N. Wang, H.-C. Sun, L. Qi et al., "Effect of stress relaxation on globe-cone seal performance with a gasket," *Vacuum*, vol. 168, Article ID 108827, 2019.

[22] G. Liu, G. Yan, and J. Yu, "Research on test method of heat transfer coefficient for refrigerator gasket," *International Journal of Refrigeration*, vol. 110, pp. 106–120, 2020.

[23] K. Rashnoo, M. J. Sharifi, M. Azadi, and M. Azadi, "Influences of reinforcement and displacement rate on microstructure, mechanical properties and fracture behaviors of cylinder-head aluminum alloy," *Materials Chemistry and Physics*, vol. 255, Article ID 123441, 2020.

[24] D. Wang, J. Wang, S. Ding, and H. Chu, "Study on evaporation heat transfer performance of composite porous wicks with spherical-dendritic powders based on orthogonal experiment," *International Journal of Heat and Mass Transfer*, vol. 156, 2020.

[25] R. T. Steinbakk, P. Ulleberg, F. Sagberg, and K. I. Fostervold, "Analysing the influence of visible roadwork activity on drivers' speed choice at work zones using a video-based experiment," *Transportation Research Part F: Traffic Psychology and Behaviour*, vol. 44, pp. 53–62, 2017.

[26] H. Ni, J. Zhang, S. Lv, X. Wang, Y. Zhu, and T. Gu, "Preparation and performance optimization of original aluminum ash coating based on plasma spraying," *The Coatings*, vol. 9, no. 11, 2019.

[27] K. Li, W. Yao, Y. Xie et al., "A strongly hydrophobic and serum-repelling surface composed of CrN films deposited on laser-patterned microstructures that was optimized with an orthogonal experiment," *Surface & Coatings Technology*, vol. 391, 2020.

[28] L. Shu, B. Wang, and Y. He, "Optimization of process parameters of laser cladding 304L alloy powder based on orthogonal experiment," vol. 1, no. 9, 2020.

[29] F. Tao, P. Gu, and Y. Yang, "Study on influencing factors of mechanical properties of ceramsite foam concrete based on orthogonal test," *Mechanical Engineering Science*, vol. 768, 2020.

[30] S. Subramani, R. Govindasamy, and G. L. N. Rao, "Predictive correlations for NOx and smoke emission of DI CI engine fuelled with diesel-biodiesel-higher alcohol blends-response

surface methodology approach," *Fuel*, vol. 269, Article ID 117304, 2020.

[31] P. Nagasankar, P. Gurusamy, S. Gopinath, K. Gnanaprakash, and G. Pradeep, "Optimization of process parameters on engine exhaust valves using Taguchi method in friction welding process," *Materials Today: Proceedings*, 2020.

[32] P. V. de Campos Souza, "Fuzzy neural networks and neuro-fuzzy networks: a review the main techniques and applications used in the literature," *Applied Soft Computing*, vol. 92, Article ID 106275, 2020.

[33] D. Deshwal, P. Sangwan, and D. Kumar, "A language identification system using hybrid features and back-propagation neural network," *Applied Acoustics*, vol. 164, Article ID 107289, 2020.

[34] H. Wang, Z. Zhang, and L. Liu, "Prediction and fitting of weld morphology of Al alloy-CFRP welding-rivet hybrid bonding joint based on GA-BP neural network," *Journal of Manufacturing Processes*, 2020, In press.

[35] G. Ma, Y. Zhang, C. Cheng, B. Zhou, P. Hu, and Y. Yuan, "Remaining useful life prediction of lithium-ion batteries based on false nearest neighbors and a hybrid neural network," *Applied Energy*, vol. 253, Article ID 113626, 2019.

[36] J. Chen, D. Jiang, Y. Zhang, and P. Zhang, "Emotion recognition from spatiotemporal EEG representations with hybrid convolutional recurrent neural networks via wearable multi-channel headset," *Computer Communications*, vol. 154, pp. 58–65, 2020.

[37] T. Baklacioglu, O. Turan, and H. Aydin, "Dynamic modeling of exergy efficiency of turboprop engine components using hybrid genetic algorithm-artificial neural networks," *Energy*, vol. 86, pp. 709–721, 2015.

[38] H. Jiang, Z. Xi, A. Rahman, and X. Zhang, "Prediction of output power with artificial neural network using extended datasets for Stirling engines," *Applied Energy*, vol. 271, Article ID 115123, 2020.

[39] J. L. S. Fagundez, T. D. M. Lanzanova, M. E. S. Martins, and N. P. G. Salau, "Joint use of artificial neural networks and particle swarm optimization to determine optimal performance of an ethanol SI engine operating with negative valve overlap strategy," *Energy*, vol. 204, Article ID 117892, 2020.

[40] Z. Chen, X. Yuan, M. Sun, J. Gao, and P. Li, "A hybrid deep computation model for feature learning on aero-engine data: applications to fault detection," *Applied Mathematical Modelling*, vol. 83, pp. 487–496, 2020.

[41] Z. Cui, S. Zhong, and Z. Yan, "Fuel savings model after aero-engine washing based on convolutional neural network prediction," *Measurement*, vol. 151, Article ID 107180, 2020.

[42] D. Miao and S. Hossain, "Improved gray wolf optimization algorithm for solving placement and sizing of electrical energy storage system in micro-grids," *ISA Transactions*, vol. 102, pp. 376–387, 2020.

[43] D. Miao, W. Chen, W. Zhao, and T. Demsas, "Parameter estimation of PEM fuel cells employing the hybrid grey wolf optimization method," *Energy*, vol. 193, Article ID 116616, 2020.

[44] Y. Dong, J. Liu, Y. Liu et al., "A RBFNN & GACMOO-based working state optimization control study on heavy-duty diesel engine working in plateau environment," *Energies*, vol. 13, no. 1, p. 279, 2020.

[45] E. Ileri, A. D. Karaoglan, and S. Akpinar, "Optimizing cetane improver concentration in biodiesel-diesel blend via grey wolf optimizer algorithm," *Fuel*, vol. 273, 2020.

[46] P. K. Gujarathi, V. A. Shah, and M. M. Lokhande, "Grey wolf algorithm for multidimensional engine optimization of converted plug-in hybrid electric vehicle," *Transportation Research Part D: Transport and Environment*, vol. 63, pp. 632–648, 2018.

[47] S. Dai, D. Niu, and Y. Han, "Forecasting of power grid investment in China based on support vector machine optimized by differential evolution algorithm and grey wolf optimization algorithm," *Applied Science*, vol. 8, no. 4, 2018.

[48] K. Luo, "Enhanced grey wolf optimizer with a model for dynamically estimating the location of the prey," *Applied Soft Computing*, vol. 77, pp. 225–235, 2019.

[49] R. K. Vijay and S. J. Nanda, "A quantum grey wolf optimizer based declustering model for analysis of earthquake catalogs in an ergodic framework," *Journal of Computational Science*, vol. 36, Article ID 101019, 2019.

[50] J. Xudong, W. Qingchun, and R. Weiping, "High-wer dieselengine's alletal cylinder gasket," 2016.

[51] W. Lei, X. Yang, X. Fang et al., "High-ressure oil pump for heavyuty diesel engine," 2014.

[52] A. P. Singh, N. Sharma, D. P. Satsangi, and A. K. Agarwal, "Effect of fuel injection pressure and premixed ratio on mineral diesel-methanol fueled reactivity controlled compression ignition mode combustion engine," *Journal of Energy Resources Technology Transactions of the ASME*, vol. 142, no. 12, 2020.

[53] J. F. Hair, G. T. M. Hult, C. M. Ringle, and M. Sarstedt, "Aprimer on partial least squares structural equation modeling(PLS-SEM)," 2014.

[54] J. Shen, M. D. Petkova, F. Liu, and C. Tang, "Toward deciphering developmental patterning with deep neural network," 2018.

[55] L. Xiao, Z. Liu, Y. Zhang, Y. Zheng, and C. Cheng, "Degradation assessment of bearings with trend-reconstruct-based features selection and gated recurrent unit network," *Measurement*, vol. 165, Article ID 108064, 2020.

[56] G. E. Hinton and R. R. Salakhutdinov, "Reducing the dimensionality of data with neural networks," *Science*, vol. 313, no. 5786, pp. 504–507, 2006.

[57] C. H. Tong, P. Furgale, and T. D. Barfoot, "Gaussian Process Gauss-Newton for non-parametric simultaneous localization and mapping," *The International Journal of Robotics Research*, vol. 32, no. 5, pp. 507–525, 2013.

[58] E. Emary, H. M. Zawbaa, and A. E. Hassanien, "Binary grey wolf optimization approaches for feature selection," *Neurocomputing*, vol. 172, no. 8, pp. 371–381, 2016.

[59] D. Karaboga and B. Basturk, "A powerful and efficient algorithm for numerical function optimization: artificial bee colony (ABC) algorithm," *Journal of Global Optimization*, vol. 39, no. 3, pp. 459–471, 2007.

[60] Z. Xue, Y. Zhang, C. Cheng, and G. Ma, "Remaining useful life prediction of lithium-ion batteries with adaptive unscented kalman filter and optimized support vector regression," *Neurocomputing*, vol. 376, pp. 95–102, 2020.